Steps towards fully nonlinear simulations of arrays of OWSC

Steps towards fully nonlinear simulations of arrays of OWSC

Gerrit Olbert[*], **Pal Schmitt**[†]
[*] TU Harburg, Hamburg/Germany, [†]Queen's University Belfast
gerrit.olbert@tu-harburg.de

1 Introduction

OWSCs in waves reflect, refract and radiate waves in different directions depending on geometrical, structural and dynamic properties of the flap. Array interaction describes the changes induced on the excitation of flaps in an array compared to the excitation of a single flap.
Renzi and Dias, 2013, Renzi et al., 2014, investigated array effects of OWSCs using a linearised semi-analytical and a linearised FEM method. However, research suggests that the applicability of linear methods for the simulation of OWSCs is limited to very small flap angles (Crooks et al., 2014, Crooks et al., 2016). Linear inviscid assumptions seem to break down in typical operating conditions (Folley et al., 2004, Asmuth et al., 2014).
It can therefore be assumed that the accuracy of linear methods in predicting the characteristic wave pattern around a flap and the interaction between multiple such devices is limited when applied to realistic operating conditions with typical pitch motion amplitudes.
Although RANS CFD tools have been shown to reproduce the motion of single flaps in waves within the levels of experimental accuracy and can provide detailed data of all field variables like surface elevation, pressure or velocity (Schmitt and Elsässer, 2015a), the simulation of arrays of WECs remains an open challenge. Due to numerical dissipation water waves simulated using volume of fluid methods tend to diminish in height and require careful spatial and temporal discretisation.
The simulation of multiple moving bodies requires adaptation of the mesh and constitutes a considerable computational effort. As with physical test facilities numerical wave tanks require non-reflecting boundary conditions and wave makers.

2 Numerical Set-Up

To save computational effort a first estimate for time step and spatial resolution is made based on two-dimensional (2D) simulations. The domain is restricted to the y and z-direction. Waves of length 1.4m and height 9mm in a water depth of 0.346m (as expected in the experimental tests) are generated by a momentum-source term wave maker (Schmitt and Elsässer, 2015b) as shown in fig. 1. The wave elevation is recorded at predefined distances from the source area. These probes are represented by vertical cylinders in figure 1.
The data collected at these probes helps to give an estimation of diffusive losses for varying spatial and time discretisation settings. Maximum time steps were varied between a 100th and 500th of the wave period. The actual timestep was set by the limiting Courant Number of 0.3 depending on the cell size. Over one wavelength the wave height decreased more than 15% for a timestep of 100th or 200th of the wave period. Limiting the time step to 500th of the wave period reduces dissipation to 7.5%.

Variations of the mesh resolution were tested for 60, 80 and 100 cells per wave length and 10, 13 and 16 cells per wave height, but with approx. only 1% seem to have little influence on numerical diffusion. The runtime is only affected by the finest temporal discretisation, in the other cases the Courant condition limits the number of timesteps. An overview of the tested settings and the corresponding total run time of a 30s simulation can be seen in table 1.

The variable C_γ, defining the magnitude of interface compression, is tested for values between 0.5 and 1.5 to assess the influence of surface compression on the numerical diffusion of waves. The results show that the resulting variance is less than 0.1% of the incident wave height. As a higher value for C_γ leads to an increased compression and therefore a sharper interface, a value of 1.0 is used for the following simulations.
An impulse source type wave maker is used to create waves, while a numerical beach is implemented using a spatially varying dissipation term (Schmitt and Elsässer, 2015b). An implementation of the three-

Fig. 1: Side view of the 2D-simulation domain, showing the momentum source wave maker (center), waveprobes (grey cylinders) and damping regions (left and right corner)

Time step Cells per λ,H	$T/100$	$T/200$	$T/500$
60, 10	16.3%	16.3%	7.5%
Runtime	2472s	2472s	7044s
80, 13	16.3%	16.3%	6.64%
Runtime	4282s	4282s	10552s
100, 16	15%	15%	6.4%
Runtime	5310s	5310s	12641s

Table 1: Diffusive losses in percent of incident wave height for different resolutions of wavelength λ and waveheight H. Losses averaged over ten periods between simulations time of $20T$ and $30T$. $T = 1$s, H = 0.009m, $\lambda \approx 1.4$m

point-reflection analysis based on wave elevation and developed by Mansard and Funke, 1980, shows that less than 1% of the incident wave is reflected at the boundaries (see fig. 2). The wave maker developed by Higuera et al., 2013, was also tested and resulted in 12% wave amplitude reflection, which is deemed too large for the purpose of array investigations.

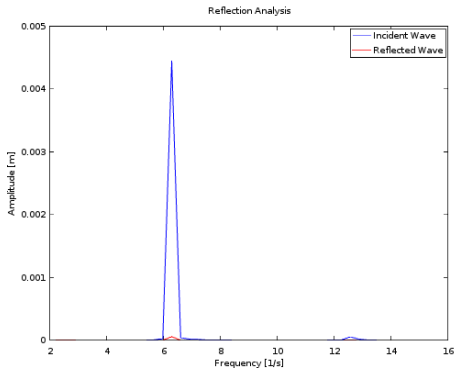

Fig. 2: Results of the three-point waveprobe analysis for $T = 1$s, $H = 0.009$m

In order to minimize the extensive computational effort required for the purpose of this investigation, an additional routine is implemented prior to 3D-simulations. The initialisation of the wave source region and the hereby induced influence on the flow field lead to oscillations in the wave height of the generated wave profile. These oscillations typically decreased to a negligible level after 30 to 40 wave periods of simulation time. Therefore, 40 wave periods of simulation time are computed in 2D. The resulting flow field is then saved and mapped onto a three-dimensional mesh, creating a long crested wave profile. Using this approach, only about 4-5 wave periods of simulation time are required prior to recording data, to allow the flow field to adapt to the presence of the flap geometries. An illustration of the mapping procedure is shown in figure 3.

(a) Side View of 2D-domain

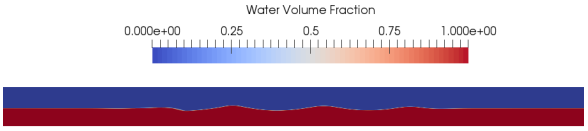

(b) 3D view on stretched 2D-domain

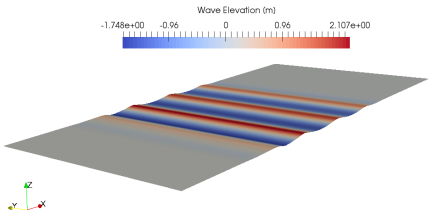

(c) 3D-domain after mapping, $t = 0$

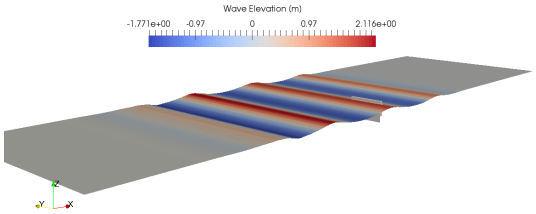

(d) 3D-domain at $t = 15T$

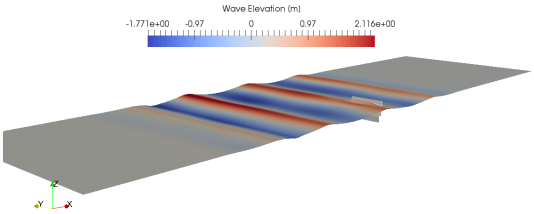

Fig. 3: Process of mapping the flow field beneath surface waves from a two-dimensional domain onto a three-dimensional grid. The 2D-grid is stretched until the lateral cell dimension corresponds to the width of the 3D-domain. The interpolation onto the grid creates a long crested wave profile, initially unaffected by the presence of the flap geometries. In this example: $T = 7$s, $H = 3$m, water depth= 13m. Flap corresponds to full scale model of Oyster© 800

2.1 Mesh distortion

The simulation of an OWSC in motion within a finite-volume-method (FVM) requires a mesh motion algorithm to account for the displacement of the body in each time step. Several approaches for the simulation of moving bodes exist, such as the overset grid solution presented by Meakin, 1998, or the sliding interface solution, e.g. Hadžić et al., 2005. Schmitt, 2013, developed a mesh motion tool for the simulation of flap type wave surge converters based on sliding interfaces and a custom field condition to account for the sea floor. Both models imply additional computational costs, requiring additional interpolation procedures and precautions to ensure mass continuity, as discussed for example by Tang et al., 2003.
A faster option is the application of mesh distortion methods. Though limited to flap rotation angles of up to 40°, they seem better suited for the envisaged array studies. *OpenFOAM* offers several dynamic mesh solvers available through its *interDyMFoam* toolkit. An explanation of the algorithm behind this method can be found in Pereira and Sequeira, 2010.
The mesh distortion caused by a moving boundary is computed using the Laplace equation (1).

$$\nabla(\gamma \nabla U) = 0 \tag{1}$$

Herein γ is the diffusion coefficient or stiffness of the mesh, regulating the spatial variation of the mesh deformation

$$\gamma(r) = \frac{1}{r^m}, \tag{2}$$

wherein r represents the distance from the moving wall and m the order of the approach. U, in this context, stands for the local mesh velocity.
A linear inverse distance definition leads to a reciprocal decrease of local distortion from a moving boundary. A quadratic inverse distance definition, in which the diffusivity is proportional to $1/l^2$, with l as

the distance to a selected boundary, results in a decrease of mesh distortion close to the boundary but leads to a larger overall number of distorted cells (see figures 4a, 4b and 4c, 4d) (Pereira and Sequeira, 2010).

As the Laplacian equation tends to show deficits for rotating deformations, a second approach will

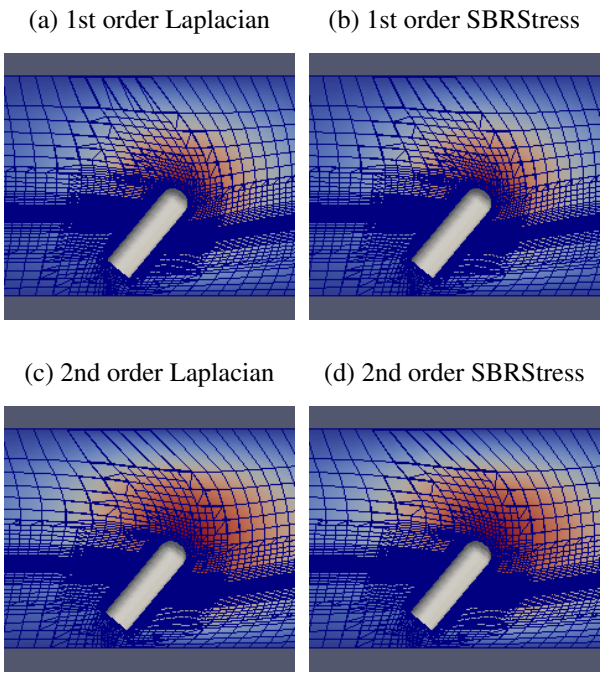

Fig. 4: Mesh distortion for first and second order approaches of Laplacian and SBRStress inverse distance diffusivity

be tested for both first and second order. The SBRStress mesh solver was developed to compute mesh deformation for rotating solid bodies and takes into account deformation due to shear while the laplace solver is based on translation (Dwight, 2006). Both approaches maintain valid meshes for flap angles $< 43°$.

3 First results

First simulations were run to compare a single flap with two, three or infinite number of devices. The devices are spaced on a line along the hinge, with one flap width distance in between. The infinite configuration was created using a symmetry condition on both laterally confining walls. Figures 5 $a - d$ show the different configurations and the surface elevation for waves of 11s period. The changes to the wave pattern are clearly visible when compared to the single flap case. These changes will be analysed and quantified in more detail in future work. To assess the array interaction, the interaction parameter q, defined as:

$$q = \frac{P'}{MP_s}, \tag{3}$$

with P' as the overall power output of the array, M as the number of devices in the array and P_s as the power output of a single device, is often used. Figure 6 shows the interaction factor for waves of 1m height over varying wave periods. The linear solution is plotted in lines, CFD results are only available for several points, due to constraints on computational power. Both datasets indicate that array interaction is positive for waves around 7s period and negative for longer waves. CFD results differ significantly from the linear solution for some periods or configurations, the exact cause will be investigated in future work.

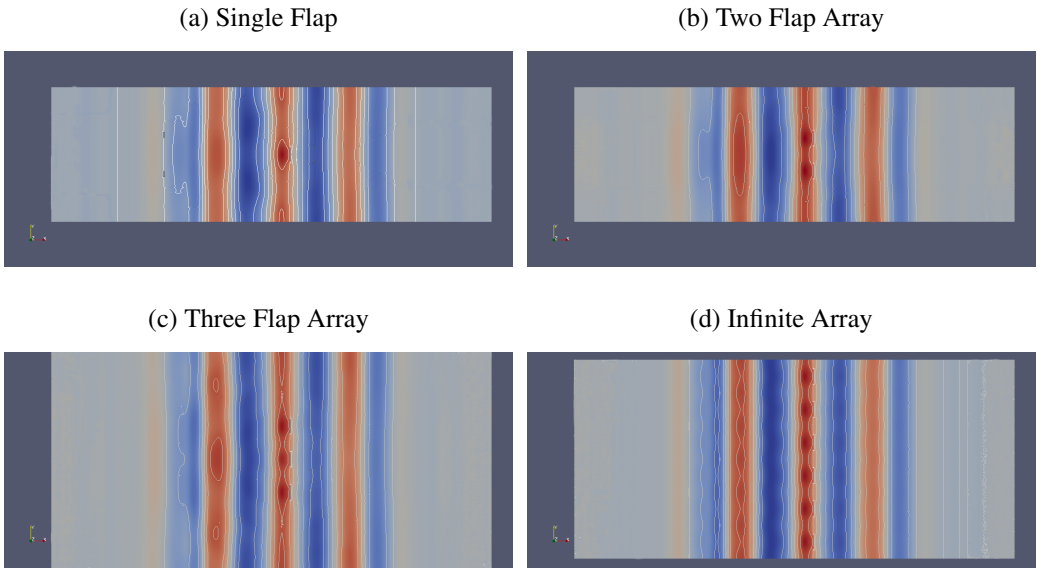

Fig. 5: Surface elevation after 605s for a single flap and three array configurations. Damping settings were defined in accordance with Renzi et al., 2014. $T = 11$s, $H = 1$m

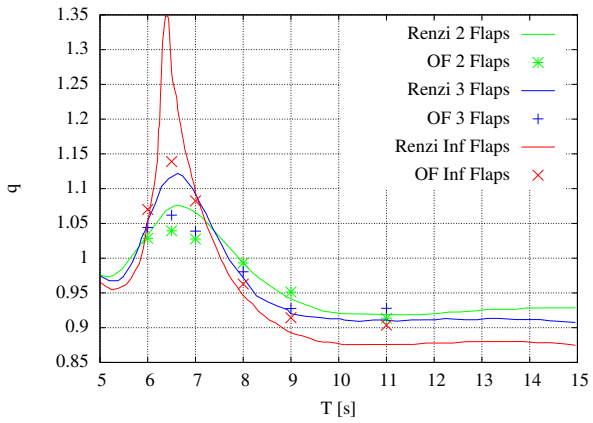

Fig. 6: Interaction factor q by Renzi (lines) in comparison to *OpenFOAM* results (points)

4 Conclusion

Careful testing and choice of appropriate mesh and timestep resolution is required for the correct application of VoF RANS simulations to the investigation of WEC arrays. First results show siginificant differences when compared to linear potential simulations, even higher deviations are expected for future simulations of more realistic sea states with wave heights of of up to three meters.

Acknowledgements

We thank the STG for funding Gerrit Olberts participation in NuTTS 2016 and the research team at Queen's University Belfast for their support in the course of this research.

References

Asmuth, H., Schmitt, P., and Henry, A.and Elsaesser, B. (2014). Determination of non-linear damping coefficients of bottom-hinged oscillating wave surge converters using numerical free decay tests. In Soares, G., editor, *Renewable Energies Offshore*. Taylor & Francis Group, London.

Crooks, D., van't Hoff, J., Folley, M., and Elsässer, B. (2016). Oscillating wave surge converter forced oscillation tests. In *Proceedings of the ASME 2016 35th International Conference on Ocean, Offshore and Arctic Engineering*.

Crooks, D., Whittaker, T. J., van't Hoff, J., and Cummins, C. (2014). Experimental validation of numericaly generated wave excitation torque on an owsc. In Soares, G., editor, *Renewable Energies Offshore*. Taylor & Francis Group, London.

Dwight, R. P. (2006). Robust mesh deformation using the linear elasticity equations. In *Proceedings of the Fourth International Conference on Computational Fluid Dynamics (ICCFD 4)*.

Folley, M., Whittaker, T., and Osterried, M. (2004). The oscillating wave surge converter. In *Proceedings of the 14th International Conference on Ocean and Polar Engineering, ISOPE 2004*.

Hadžić, I., Hennig, J., Perić, M., and Xing-Kaeding, Y. (2005). Computation of flow-induced motion of floating bodies. *Applied Mathematical Modelling*, 29(12):1196 – 1210.

Higuera, P., Lara, J. L., and Losada, I. J. (2013). Realistic wave generation and active wave absorption for navier-stokes models: Application to OpenFOAM. *Coastal Engineering*, 71(0):102 – 118.

Mansard, E. and Funke, E. (1980). The measurement of incident and reflected spectra using a least square method. In *ICCE'80*, pages 154–172. ASCE.

Meakin, R. L. (1998). *Handbook of Grid Generation*. CRC Press, Boca Raton.

Pereira, J. C. F. and Sequeira, A., editors (2010). *Dynamic Mesh Handling In Openfoam Applied To Fluid-structure Interaction Simulations*, European Conference on Computational Fluid Dynamics.

Renzi, E., Abdolali, A., Bellotti, G., and Dias, F. (2014). Wave-power absorption from a finite array of oscillating wave surge converters. *Renewable Energy*, 63:55 – 68.

Renzi, E. and Dias, F. (2013). Relations for a periodic array of flap-type wave energy converters. *Applied Ocean Research*, 39:31 – 39.

Schmitt, P. (2013). *Investigation of the near flow field of bottom hinged flap type wave energy converters*. PhD thesis, Queen's University Belfast.

Schmitt, P. and Elsässer, B. (2015a). On the use of OpenFOAM to model oscillating wave surge converters. *Ocean Engineering*, 108:98 – 104.

Schmitt, P. and Elsässer, B. (2015b). A review of wave makers for 3d numerical simulations. *MARINE 2015 - Computational Methods in Marine Engineering VI*, pages 437–446.

Tang, H., Jones, S. C., and Sotiropoulos, F. (2003). An overset-grid method for 3d unsteady incompressible flows. *Journal of Computational Physics*, 191(2):567 – 600.